Published in final edited form as:
Soft Matter. 2014 February 28; 10(8): 1142–1150. doi:10.1039/c3sm51943k.

Formation and Mechanical Characterization of Ionically Crosslinked Membranes at Oil/Water Interfaces

Wa Yuan, **Evan J. Laprade**, **Kevin J. Henderson**, and **Kenneth R. Shull**

Abstract

Here we report on the preparation and mechanical characterization of a 2-D self assembled membrane formed by ionically crosslinking the polyelectrolyte parts of a gradient amphiphilic copolymer at oil and water interfaces. To fabricate these membranes, chloroform solutions of styrene/acrylic acid copolymers were suspended as pendant drops in an aqueous embedding phase. Due to the amphiphilic nature of these molecules, the copolymer chains migrate to the oil/water interface creating an interfacial layer. Upon the addition of zinc acetate to the embedding phase, crosslinks between copolymer molecules are formed via zinc-carboxylate complexes. While ionically crosslinked block copolymer membranes were critically damaged after one expansion cycle, ionically crosslinked gradient copolymers formed durable membranes that maintained their physical integrity through multiple expansion-compression-expansion cycles. This difference in mechanical behavior is attributed to the fact that gradient copolymer are more effective interfacial modifiers and have a significantly different molecular alignment at the oil/water interface. Additionally by changing the incubation time from 20 to 30 minutes, the low-strain dilatational modulus of these membranes was significantly increased due to higher interfacial coverage and crosslinking density. Longer incubation times also led to a distinct yield point and plastic deformation behavior at larger strains. Further mechanical characterization of the membranes showed that they can be quite robust and that by replacing the internal oil phase with an aqueous solution, future testing of membrane filtration and permeation may be possible.

1 Introduction

Ionically crosslinked networks are often incorporated into covalently crosslinked polymers to enhance their mechanical and transport properties [1, 2, 3]. In polymer bulk gels for instance, the addition of a second, tightly cross-linked network assists in broadening the fracture zone and maximizing dissipation, creating soft materials with fracture energies comparable to or exceeding that of natural biomaterials [1]. Additionally, the reversibility of these bonds provides these gels with a remarkable ability to recover after plastic deformation, giving them a self-healing character [2]. Ionic crosslinking of two dimensional structures is equally attractive, as it can be used to tailor membrane permeability and permaselectivity for liquid phase transport applications. In recent work, these films have increasingly been targeted as membranes for liquid mixture separations [4, 5], drug delivery [6], and fuel cells [7, 8, 9]. Looking towards these goals, we introduce a simple way of preparing and mechanically characterizing free standing ionically crosslinked polymer membranes.

The most frequently used technique to produce ionic crosslinking is by complexation of multi-valent cations and carboxylate ligands, in what is predominantly an electro-static interaction. In our experiments, pendant drop membranes were formed through zinc (II) crosslinking of amphiphilic stryene-acrylic acid gradient copolymer (Figure 2) at an oil/water interface as shown in Figure 1. The pendant drop technique is a commonly used method for characterizing the mechanical properties of two dimensional structures that self-assemble at fluid-fluid interfaces. While conceptually more complex than flat interface techniques [10, 11, 12], a pendant drop technique can offer several important advantages due its small reagent volumes and rapid equilibration times. The interfacial tension between the drop and embedding phase can be obtained by analyzing the drop shape, and changing the drop volume allows one to mechanically characterize the interface.

The amphiphilic copolymer used here to form crosslinked membranes are referred to as gradient copolymers (Figure 2). They possess a gradual change of composition along the backbone [13], which leads to lower repulsion forces distributed along the chain. It has been shown previously that the molecular structure of gradient copolymers results in a larger critical micelle concentration in polymer blends [14, 15, 16] and molecular alignment at oil/water interface that differs significantly from traditional block copolymers [17]. Our work suggests that copolymer membrane formation is facilitated by the reduction of these kinetic barriers and by the specific details of the molecular organization at the interface before crosslinking.

In this paper we begin by discussing the materials and methods for fabricating ionically crosslinked pendant drops. Then we summarize the mechanics of the pendant drop geometry, and provide the background necessary to analyze both fluid and elastic interfaces. Next we model an ionically crosslinked drop with both analyses, evaluating the fit quality and principal tension predictions. The availability of these models puts us in a position to characterize the mechanical behavior of these membranes, look at the effect of processing conditions, and discuss their self-healing ability. Lastly we present preliminary results highlighting how the robust nature of this technique could be used to look at transport through these crosslinked interfaces.

2 Materials and Methods

2.1 Materials

Styrene/acrylic acid (S/AA) gradient copolymers were synthesized as previously described[17] using semi-batch nitroxide mediated controlled radical polymerization (NM-CRP) from unimolecular initiator alkoxyamine 29 (2,2,5-trimethyl-3-(1-phenylethoxy)-4-phenyl-3-azahexane)[18]. The PS/PtBA precursor copolymers were recovered by cycles of precipitation into methanol and dissolution into tetrahydrofuran before drying under vacuum. For comparison a block copolymer with similar molecular weight was also prepared, using sequential, batch NM-CRP. The final products were labeled as G92 (M_n = 91,800 g/mol, styrene fraction = 0.55) and B89 (M_n = 88,700 g/mol, styrene fraction = 0.69), according to the copolymer type and number average molecular weight. The final apparent molecular weights (MWs) and cumulative styrene mole fraction (FS) for the two types of

copolymers used for this study are summarized in table 1. Both copolymers were dissolved in chloroform (CHROMASOLV PLUS, FOR HPLC) at a concentration of 0.02 mg/mL.

Dihydrate zinc acetate (as received, Sigma Aldrich) and pure water (A.C.S. REAGENT, Sigma Aldrich) were used to prepare 400 mM zinc acetate solutions. These solutions were buffered with acidic acid to a final pH of 6, confirmed using a WTW Portable pH Tester, Model 20.

2.2 Drop Shape Analysis System

A commercial drop shape tensiometer (Krüss DSA 100) was used to image the pendant drop profile. Drop shape analysis video was analyzed with a custom written MATLAB (Mathworks) pendant drop mechanical analysis, outlined in section 3. Drop volume was controlled via a motor driven syringe system.

2.3 Pendant Drop Membrane Fabrication

Interfacial layers were investigated using the pendant drop method and drop-shape analysis (DSA). A ~4-6μl pendant drop of chloroform containing the desired copolymer was formed at the end of capillary needle (diameter = 0.914 mm) inside a water filled glass cuvette (cuvette dimensions =1 cm × 1 cm × 5 cm). Once the pendant drop was formed, it was fixed at the initial volume for a period of time (referred to here as the "incubation period") to allow the copolymers to migrate to the oil and water interface. After this incubation period, zinc acetate solution was added to the aqueous imbedding phase to create carboxylate ligand complexation at the interface. Final concentration of zinc acetate in the aqueous phase was approximately 40 mM. After the addition of zinc acetate, the drop was held for approximately five minutes to form an ionically crosslinked interface. Immediately following this period, the drop volume was decreased slightly to test the formation of the membrane, indicated by wrinkling of the interface.

After the drop was re-expanded back to the original size, a set of cycles were carried out following a routine of expansion-compression-expansion. Drops were expanded to a ~40% increase in interfacial area (relative to the initial drop surface area), compressed to a ~20% reduction, and then re-expanded back to the original size. The time between the end of one expansion-compression-expansion cycle and the start of the next was approximately three minutes. All experiments were performed at a fixed flow rate of 0.4 μL/min. Before and after each new experiment, the glass cuvette was thoroughly washed with acetone and water, while the needles and glass syringe were washed with acetone and chloroform.

Figure 3 shows representative images at different stages of expansion and compression for a crosslinked G92 copolymer membrane. We note that the wrinkling wavelength observed during compression is approximately 35-40 μm for the smallest observable wrinkles, and at larger compressions these small wrinkles became larger folds with a wavelength of approximately 100 μm. These wrinkle wavelengths are quite similar to those observed by Erni *et al.* [19] for oil/water emulsion drops exhibiting shear elasticity.

3 Membrane Mechanics

3.1 Theoretical Background

DSA is most commonly used to measure the interfacial tension between two immiscible fluids, but has increasingly been employed to characterize the mechanical behavior of molecular structures that self-assemble at these interfaces [19, 20, 21, 22, 23]. General theoretical frameworks that encompass these solid-like interfaces have been summarized recently [24, 25]; here we follow the formulation given by Carvajal *et al.* [25].

In Figure 4, we define a coordinate system for the pendant drop geometry with it's origin at the drop apex. The arc length of the interface between the two phases, s, runs from the apex ($s = 0$) to the capillary edge ($s = l$), where l is the total integrated arc length. The shape of the pendant drop interface is defined by its principal curvatures R_ξ and R_φ, the curvatures in the r - z plane and in the azimuthal direction respectively. The principal curvatures are defined as

$$R_\xi = \frac{ds}{d\alpha} \quad (1)$$

$$R_\phi = \frac{r}{\sin\alpha} \quad (2)$$

where the quantity $\alpha(s)$ is the angle between the tangent to the interface at $[r(s), z(s)]$ and the radial axis.

In the most general case of an elastic or solid-like interface, the pendant drop geometry is governed by force balances in the direction normal to the interface, and along the ξ principal direction. (a force balance in the φ direction is satisfied by the axisymmetry of the problem). From the normal force balance one can derive the Young-Laplace relation:

$$\Delta P = \frac{T_\xi}{R_\xi} + \frac{T_\phi}{R_\phi} \quad (3)$$

where the principals tensions, T_ξ and T_φ, and local curvatures balance the pressure difference across the interface, ΔP. It can be shown that the mechanical equilibrium equation for the ξ direction is given by:

$$\frac{d}{dr}(T_\xi r) = T_\phi \quad (4)$$

In the case of a purely fluid interface, which is unable to support shear stresses, the principal tensions are spatially uniform and equal, $T_\xi = T_\varphi = \gamma$. Equation 4 is automatically satisfied, and the interfacial tension can be measured by simply fitting the Young-Laplace equation to the drop profile.

An elastic or solid interface presents a more complicated situation where the principal tensions are no longer isotropic and instead will depend on the local in-plane principal

strains, λ_ξ and λ_φ. For an elastic interface we assume that the principal tensions consist of a pretension component, γ', equal to the interfacial tension of the pendant drop in the undeformed state, and an elastic component, which is determined by the strain energy per unit area of the undeformed membrane, U.

$$T_\xi = \gamma' + \frac{1}{\lambda_\phi}\frac{\partial U}{\partial \lambda_\xi} \quad (5)$$

$$T_\phi = \gamma' + \frac{1}{\lambda_\xi}\frac{\partial U}{\partial \lambda_\phi} \quad (6)$$

A neo-Hookean strain energy function is commonly chosen as a general description of elasticity[26], and here we use it to derive the following expressions for the principal tensions:

$$T_\xi = \gamma' + \frac{Eh_0}{3}\left(\frac{\lambda_\xi}{\lambda_\phi} - \frac{1}{\lambda_\xi^3 \lambda_\phi^3}\right) \quad (7)$$

$$T_\phi = \gamma' + \frac{Eh_0}{3}\left(\frac{\lambda_\phi}{\lambda_\xi} - \frac{1}{\lambda_\xi^3 \lambda_\phi^3}\right) \quad (8)$$

where Eh_0 is the low-strain dilatational modulus, E is Young's elastic modulus, and h_0 is the undeformed thickness of the membrane. Equations (7,8) were derived under the assumption of incompressibility.

In section 3.4 we utilize both the fluid interface analysis (equation 3) and the elastic interface analysis (equations 3-8) to characterize the mechanical behavior of a crosslinked gradient copolymer pendant drop.

3.2 Fluid Interface Fitting

Isotropic interfacial tension values were determined using a modified version of the Young-Laplace fitting routine previously described by Carvajal *et al.* [25]. To briefly summarize, equations (1-3) are combined with the geometrical relations $dr/ds = \cos\alpha$ and $dz/ds = \sin\alpha$, to give three coupled first order differential equations (for α, r, and z) that describe the pendant drop's configuration. We specify five boundary conditions: three at the drop apex and two at the capillary needle edge. In order for all five boundary conditions to be met, two parameters must be allowed to float. These parameters are the interfacial tension, γ, and the pressure at the apex, P_0. A custom MATLAB script was used to digitize the drop profile, solve the differential equations, and adjust the parameters to determine which value of γ minimizes the error, Λ_{res},in profile fitting. This error is defined in the following way:

$$\Lambda_{res} = \frac{1}{NR_m}\sum_{i=1}^{N} d_i, \quad (9)$$

where d_i is the normal distance between the model and experimental profile at each model profile point ($r(i)$, $z(i)$), R_m is the radius of the membrane holder, and N is the total number of points along the profile. Note that Λ_{res} is the average distance between the actual drop profile and the fit to the droplet shape from the solution to the equations in the previous section, normalized by R_m.

3.3 Elastic Interface Fitting

For the elastic case we need to solve a total of four differential equations, for α, z, λ_ξ, and λ_φ. There are a total of six boundary conditions to be met, so two parameters must be allowed to float, and these parameters are the pressure at the apex of the deformed membrane, and Eh_0, the low strain dilatational modulus. Our use of Eh_0 as an adjustable parameter is not a rigorous treatment of viscoelasticity, but this method provides a simple first order approximation of the time-dependent modulus of the membranes.

To analyze an elastic interface we make the assumption that a pendant drop with a liquid–like interfacial layer has undergone crosslinking, forming an elastic membrane at the interface. This undeformed, yet crosslinked pendant drop is defined as the reference configuration. It is assumed that in this undeformed state, the principal tensions are spatially uniform and equal to one another, $T_\xi = T_\varphi = \gamma'$. Subsequent deformation of the drop changes the local values of λ_ξ and λ_φ and therefore the elastic contributions to the principal tensions. We begin by determining γ, analyzing an image of the undeformed drop with the fluid interface analysis. After determining γ', the elastic drop analysis can be used to model the deformation of drop starting with expansion. A custom MATLAB script was used to digitize the drop profile, solve the differential equations, and adjust the parameters to minimizes the error, Λres.

3.4 Fluid and Elastic Interface Analysis Comparison

The fluid to elastic transition of pendant drop interfaces can be monitored by examining the error in fitting the Young-Laplace equation to the interface shape [27, 24, 22]. As the drop becomes more solid-like there will be an increase in the error that can provide a signature of the formation of an elastic interface with a non-uniform tension. Use of an approximate “fluid interface” model that assumes a uniform, isotropic tension is motivated by the simplicity of the fitting routines that are generally available on commercial pendant drop instruments. An important question that needs to be addressed in these situations is how closely this fluid interface analysis approximates the true interfacial tension. In this section we examine the agreement between the elastic and fluid interface analyses for our crosslinked pendant drops, specifically looking at the quality of the profile fits and at the magnitude and spatial variation of the interfacial tensions.

Following the procedure outlined in sections 3.2 and 3.3, fluid and elastic interface analyses were applied to the expansion and compression cycle of a G92 gradient copolymer pendant drop. During the 20 minute incubation period, the drop interface has fluid-like character, and we expect excellent agreement between the interface shape and the Young-Laplace solution. We can use the average value of the fitting error in this regime ($\Lambda_{res} = 0.0025$), as a reference for what constitutes a quality fit. In Figure 5, this average fitting error for the

uncrosslinked drop is plotted as a solid black line, along with the fitting error for the fluid and elastic interface analyses during the expansion and compression of the crosslinked G92 gradient copolymer pendant drop. Both analyses produce comparable residuals over the majority of deformations. In both cases the error is comparable to our reference value until the drop is compressed back to an areal dilatation of $A/A_0 = 1$, where A is the actual interfacial area and A_0 is the original interfacial area for that specific cycle. Further compression results in poor fitting for both cases, particularly as the membrane begins to wrinkle ($A/A_0 < 0.95$), and the fitting error sharply increases. As neither model correctly interprets the tensions in this regime, we restrict our analysis to $A/A_0 > 0.95$ in the work that follows.

The profile fits and local residuals at interfacial area extensions $A/A_0 = 1.09$ (time=110s) and $A/A_0 = 1.29$ (time=548s) are shown in Figures 6(a,c) and (d-f) respectively. For both of these deformations the fluid interface, elastic interface, and experimental profiles are nearly indistinguishable from one another (Figure 6(a,d)) and small differences only become clear when looking at the local residuals (Figure 6(b,e)). More significant differences between the models are evident in the principal tension behavior, Figure 6(c,f), particularly in the spatial distribution of the principal tensions. The additional boundary conditions for the elastic interface analysis lead to an anisotropic strain state, with the boundary condition $\lambda_\xi(s = 0) = \lambda_\varphi(s = 0)$ forcing equibiaxial tension at the drop apex and the boundary condition $\lambda_\varphi(s = l) = 1$ diverging the principal tensions at the capillary edge.

Our analysis of the G92 crosslinked interface shows a small deviation between the elastic tensions and γ, as depicted in Figures 7 and 8. Interestingly, despite the very close agreement between the fluid and elastic profile shape, the interfacial tension, g, does not necessarily fall somewhere in between the predictions for T_ξ and T_φ. At the apex, the fluid analysis slightly overestimates the tension, as shown in Figure 7, and similarly overestimates T_φ at the capillary edge, as shown in Figure 8. The best agreement between the fluid and elastic analysis can be found in their prediction of T_ξ at the capillary edge, where the tensions track closely until $A/A_0 \approx 1.08$, at which point the fitting error for both analyses begins to significantly increase.

While the deviations between the elastic and fluid interface analyses are non-trivial, good agreement exists between the two, particularly for γ and T_ξ at $z = \delta$. These observations suggest that in our case, the simpler, and more tractable fluid analysis can provide a useful approximation of the interfacial tension. For more strongly crosslinked interfaces with higher stiffness and less healing capability, [24] one would expect the deviations between the elastic and fluid fitting routines to be more pronounced. We used the fluid model to analyze all of the data discussed in the following sections.

4 Results and Discussion

4.1 Block and Gradient Copolymer Membrane Deformation

As described above, the G92 gradient copolymer was dissolved in chloroform at a concentration of 0.02 mg/mL, and this solution was used to form a pendant drop at the tip of a capillary needle submerged in water. During the incubation period the interfacial tension

decreased significantly from that of pure chloroform/water (32.8 mN/m). After a 20 minute incubation period γ decreased approximately 17 mN/m, and after a 30 minute incubation period γ decreased approximately 22 mN/m. Additionally during this incubation time, the initially clear drop became more cloudy in appearance. After the addition of zinc acetate, the G92 drop was compressed and wrinkling was clearly observed, indicating the formation of a crosslinked membrane at the oil/water interface. On each subsequent expansion/compression cycle wrinkling was always observed during compression. Figure 9 shows shows a comparison between a expansion-compression cycle of interfaces with and without cross-linking by exposure to zinc acetate.

Droplets formed by B89 on the other hand showed a significantly smaller decrease in interfacial tension within these incubation periods compared to G92 gradient copolymer. This observation was consistent with our previous results which showed that in a limited time scale block copolymers are less efficient at going to the oil/water interface due to kinetic barriers associated with micelle aggregation in the chloroform phase Yuan *et al.* [17]. The coverage of copolymers at the interface was not sufficient to form a uniform membrane, and thus droplets formed by B89 did not show a clear sign of wrinkling during compression. To further compare, we increased the concentration of B89 solution to 0.1mg/mL and extended the incubation time to 3 hours. Under this condition the interface did show a sign of wrinkling during the compression process, indicating the formation of crosslinked membrane. However, when we expanded the drop by 20% and re-compressed it, the wrinkling phenomenon was no longer observed, indicating damage of the membrane during expansion.

Figure 10 shows a schematic representation of the proposed cross-linking processes for the two types of copolymers. For block copolymers, the junction points between blocks of the hydrophobic and hydrophilic monomers are localized at the oil/water interface, forming a brush-like structure. Addition of zinc ions to the aqueous phase crosslinks this entangled brush layer. When the interface is expanded, a tensile force is applied to the crosslinked layer pulling the block copolymers apart, breaking the membrane. Gradient copolymers on the other hand have multiple hydrophilic/hydrophobic junction points along the chain which may result in a more “parallel” structure, with the molecules laterally extended along the interface[16, 17, 28]. After the addition of zinc these “parallel” chains form a more complex network of intermolecular cross-links, resulting in a formation of a stronger membrane. When this membrane is placed under a similar tensile force, the “parallel” molecules do not simply detach from each other, but rather extend and uncoil. This helps maintaining the physical integrity of the membrane and enables the membrane to be expanded to twice its original area.

4.2 Mechanical Characterization of Gradient Copolymer Membranes

The mechanical behavior of the G92 crosslinked membranes is not only influenced by the initial crosslinked network, but also by the adsorption/desorption of uncrosslinked copolymer, and the continuous self-healing of the carboxylate-ligand linkages. Since the pendant drop remains in an aqueous zinc rich environment it is possible for old crosslinks to repair or restructure, and for new crosslinks to form. The specific time scale for these

crosslinking events is expected to be relatively rapid, and the reproducibility of the cycling behavior suggests that the three minute gap between expansion cycles is sufficient for new crosslinks to form. The deformation shown in Figure 9 is a characteristic cycle (in this case the first cycle) for a G92 membrane incubated for 20 minutes. At small strains there is an initial linear section where we can characterize the stiffness of these membranes by measuring the dilatational modulus, κ, defined as follows:

$$\kappa = A_0 \frac{d\gamma}{dA} \quad (10)$$

The small strain stiffness for this first expansion cycle was $\kappa \approx 47$ mN/m, significantly higher than that of the uncrosslinked layer, $\kappa \approx 14$ mN/m. While the dilatational modulus remains fairly constant for the uncrosslinked interface in Figure 7, as the membrane is expanded to larger strains the slope of the interfacial tension curve decreases. Our explanation for this softening behavior is a combination of damage to the crosslinked network (local crosslink fracture, rather than catastrophic failure), and also adsorbtion of uncrosslinked copolymer to the expanded interface. As the drop is compressed back to its original size, uncrosslinked copolymer de-adsorbtion from the interface contributes to the significant hysteresis between the expansion and compression cycles. After the drop is compressed back to its original interfacial area, the three minute incubation time in between cycles allows the fractured interface to repair and for new crosslinks to form. If we consider the beginning of each cycle to be like the formation of a new crosslinked membrane, we can characterize an excess surface stress, σ, for each cycle:

$$\sigma = \gamma - \gamma' \quad (11)$$

where γ' is the interfacial tension at the beginning of each specific cycle. In Figure 11, σ is plotted as function of A/A_0 for the first four deformation cycles of the crosslinked G92 copolymer after a 20 minute incubation. The small strain expansion is comparable for all cycles, characterized by an average κ value of 45 mN/m. The reproducibility of the deformation behavior for cycles 2-4 highlights the robustness and self-healing nature of these membranes.

Alteration of the fabrication procedure, specifically the incubation time (the time between drop formation and initial crosslinking), significantly influences the mechanical properties of these membranes. Increasing the incubation time from 20 minutes to 30 minutes, leads to a higher surface coverage of gradient copolymers, evident by the lower interfacial tension at the time of initial crosslinking. The excess surface stress behavior for G92 copolymer membranes incubated for 30 minutes is shown in Figure 12. Here we see that a distinctive linear region defines initial expansion, followed by plateauing at larger extensions. Similar behavior has been described previously [21], as a linear elastic region, followed by yielding and plasticity. In the linear elastic region, $\kappa \approx 60$ mN/m, consistent with a more tightly crosslinked interface compared to the 20 minute incubation membranes. While the membranes formed from shorter incubation times experience a gradual yielding, these membranes undergo an abrupt yielding and have a well-defined stress plateau. Evidence of

possible network damage near the capillary edge was visibly observed around this transition point, supporting this yielding description. Despite this damage, a second expansion/compression follows a nearly identical trend due to the self-healing ability of these membranes.

4.3 Liquid exchange and membrane permeation

Due to the mechanical robustness of the crosslinked membrane, we were able to carry out some more complex manipulations on the interface without destroying the membrane, as shown in Figure 13(d-f). Here we use a 1:1 (weight percentage) mixed solvent of chloroform and toluene to dissolve the gradient copolymer sample, and crosslink the membrane on top of a open-end glass tube in a water embedding phase. When the crosslinked membrane was formed, a needle is inserted into the glass tube to create a bubble of water inside the mixed chloroform/toluene solvent. The water bubble initially stays on the upper part of the oil drop because of the density difference between the oil and water phases. Over the time chloroform dissolves preferentially into the embedding phase, decreasing the density of the mixed solvent. Thus the water bubble eventually sinks to the bottom and comes into contact with the the cross-linked membrane (Figure 13(g)). This allows us to create a water/membrane/water geometry, which is ideal for future tests such as permeation and filtration.

5 Conclusion

Here we demonstrated a method for ionically crosslinking amphiphilic copolymers at an oil/water interface and characterized the mechanical properties of the membranes that formed. The key results can be summarized as follows:

- Ionically crosslinked gradient copolymers formed durable membranes that maintained their physical integrity through multiple expansion-compression-expansion cycles. In contrast, ionically crosslinked block copolymer membranes were critically damaged after one expansion cycle. This result is attributed to the fact that gradient copolymer are more effective interfacial modifiers and have a significantly different molecular alignment at the oil/water interface.
- A fluid interface analysis and an elastic interface analysis were used to fit the interfacial tension of an ionically crosslinked gradient copolymer membrane. The two models had similar profile fitting errors and predicted similar trends in the interfacial tension behavior, with the closest agreement occurring in the prediction of T_{ξ} at the capillary edge. Due to the comparable results given by the models and the simplicity of the Young-Laplace fitting routine, a fluid interface analysis was used for further mechanical characterization.
- By changing the incubation time with the copolymer solution from 20 to 30 minutes, the low-strain dilatational modulus of these membranes was significantly increased due to higher interfacial coverage and crosslinking density. Longer incubation times also led to a distinct yield point and plastic deformation behavior at larger strains.

- The reproducible deformation behavior of these membranes is partially attributed to the reversible nature of ionic crosslinks which allowed these membranes to self-heal.

Acknowledgments

This work was supported by the Petroleum Research Fund, NSF MRSEC program (DMR-0520513), and the National Institutes of Health under Grant 5R37DE014193-08. Fellowship support from 3M to W. Yuan and from NSF to Kevin J. Henderson is gratefully acknowledged. We are grateful to J.M. Torkelson and M. Mok for providing the gradient copolymers.

References

1. Sun J-Y, Zhao X, Illeperuma WRK, Chaudhuri O, Oh KH, Mooney DJ, Vlassak JJ, Suo Z. Nature. 2012; 489:133–136. [PubMed: 22955625]
2. Bakarich SE, Pidcock GC, Balding P, Stevens L, Calvert P, Panhuis M. i. h. Soft Matter. 2012; 8:9985–9988.
3. Jătariu AN, Popa M, Curteanu S, Peptu CA. Journal of Biomedical Materials Research Part A. 2011; 98A:342–350. (Cadinoiu).
4. Devi DA, Smitha B, Sridhar S, Aminabhavi T. Separation and Purification Technology. 2006; 51:104–111.
5. Huang RYM, Shieh J-J. Separation Science and Technology. 1997; 32:2765–2784.
6. Don T-M, Huang M-L, Chiu A-C, Kuo K-H, Chiu W-Y, Chiu L-H. Materials Chemistry and Physics. 2008; 107:266–273.
7. Gasa JV, Weiss R, Shaw MT. Journal of Membrane Science. 2007; 304:173–180.
8. Kerres J, Zhang W, Ullrich A, Tang C-M, Hein M, Gogel V, Frey T, Jörissen L. Desalination. 2002; 147:173–178.
9. Kerres JA. Fuel Cells. 2005; 5:230–247.
10. Bos MA, van Vliet T. Advances in Colloid and Interface Science. 2001; 91:437–471. [PubMed: 11511044]
11. Boucher E, Kent H. Journal of Colloid and Interface Science. 1978; 67:10–15.
12. Cabrerizo-Vílchez MA, Wege HA, Holgado-Terriza JA, Neumann AW. Review of Scientific Instruments. 1999; 70:2438–2444.
13. Lefebvre MD, McSwain RL, Dettmer CM, Xu C, Davila JR, Composto RJ, Nguyen ST, Shull KR. Macromolecules. 2005; 38:10494–10502.
14. Leibler L, Orland H, Wheeler J. J. Chem. Phys. 1983; 79:3550.
15. Sandoval RW, Williams DE, Kim J, Roth CB, Torkelson JM. Journal of Polymer Science Part B: Polymer Physics. 2008; 46:2672–2682.
16. Shull K. Macromolecules. 2002; 35:8631–8639.
17. Yuan W, Mok MM, Kim J, Wong CLH, Dettmer CM, Nguyen ST, Torkelson JM, Shull KR. Langmuir. 2010; 26:3261–3267. [PubMed: 19968259]
18. Wong CLH, Kim J, Torkelson JM. Journal of Polymer Science Part B: Polymer Physics. 2007; 45:2842–2849.
19. Erni P, Jerri HA, Wong K, Parker A. Soft Matter. 2012; 8:6958–6967.
20. Ferri JK, Dong W-F, Miller R, Möhwald H. Macromolecules. 2006; 39:1532–1537.
21. Ferri JK, Kotsmar C, Miller R. Advances in Colloid and Interface Science. 2010; 161:29–47. [PubMed: 20810096]
22. Alexandrov NA, Marinova KG, Gurkov TD, Danov KD, Kralchevsky PA, Stoyanov SD, Blijdenstein TB, Arnaudov LN, Pelan EG, Lips A. Journal of Colloid and Interface Science. 2012; 376:296–306. [PubMed: 22480400]
23. Kang Z, Yeung A, Foght JM, Gray MR. Colloids and Surfaces B: Biointerfaces. 2008; 62:273–279.

24. Ferri JK, Fernandes PAL, McRuiz JT, Gambinossi F. Soft Matter. 2012; 8:10352–10359.
25. Carvajal D, Laprade EJ, Henderson KJ, Shull KR. Soft Matter. 2011; 7:10508.
26. Long R, Shull KR, Hui C-Y. Journal of the Mechanics and Physics of Solids. 2010; 58:1225–1242.
27. Ferri, JK.; Fernandes, PAL. Bubble and Drop Interfaces. Miller, R.; Liggieri, L.; Brill, EJ., editors. Vol. 2. Leiden, Netherlands: 2011. p. 61-74.
28. Wang R, Li W, Luo Y, Li B-G, Shi A-C, Zhu S. Macromolecules. 2011; 42:2275–2285.

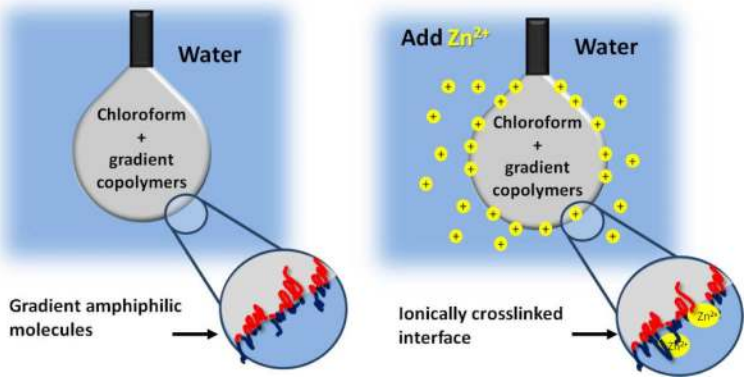

Figure 1.

Formation of ionically crosslinked interfacial layers: (a) Gradient copolymers dissolved in chloroform adsorb to the interface of a pendant drop at the tip of a capillary needle. The embedding phase is pure water. The inset shows an idealized orientation of gradient copolymers at the oil/water interface. (b) Zinc acetate solution is added to the aqueous embedding phase. The inset shows divalent ion-carboxylate ligand complexing at the interface, creating an ionically crosslinked membrane.

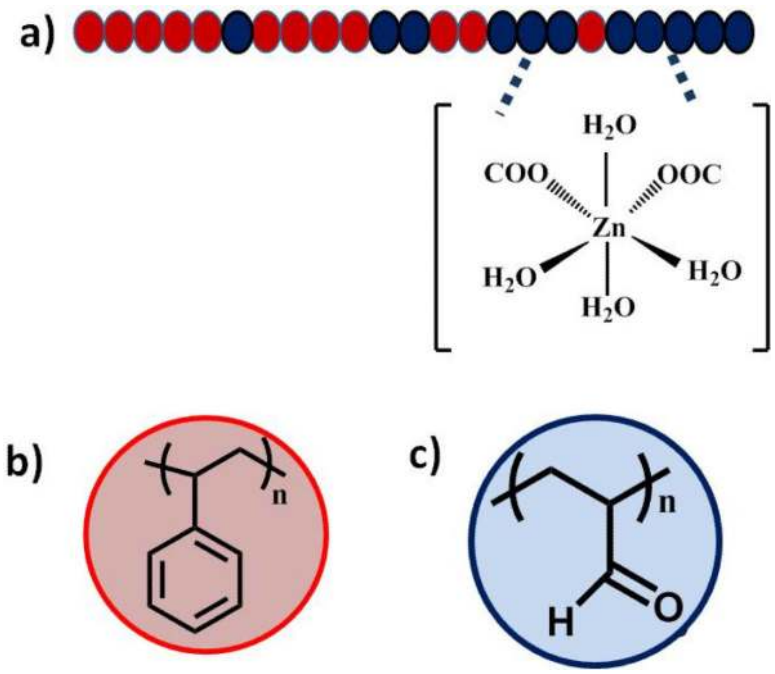

Figure 2.

(a) Schematic structure of a styrene/acrylic acid gradient copolymer. Carboxylate ligands replace aqua ligands in inner sphere of a Zn ionic complex. Schematic structure of styrene (b) and (c) acrylic acid.

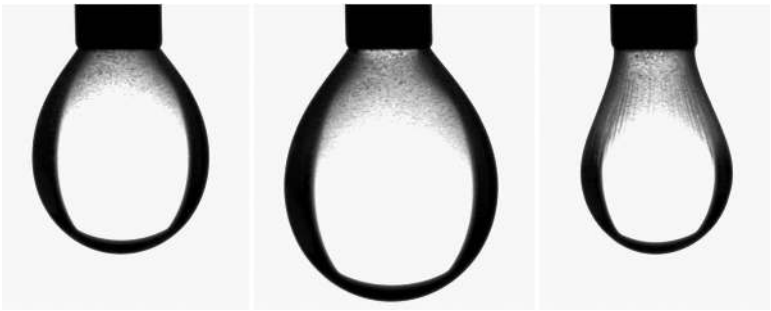

Figure 3.

Images of crosslinked G92 copolymer membrane (20 minute incubation) during the 1st expansion/compression/expansion cycle. The left image corresponds to $A/A_0=1$, where A_0 is the drop surface area at the beginning of the cycle. The center image corresponds to $A/A_0=1.39$ (maximum surface area during cycle). The right image corresponds to a deep compressed state ($A/A_0=0.81$) where wrinkling can be observed in the upper portion of drop interface.

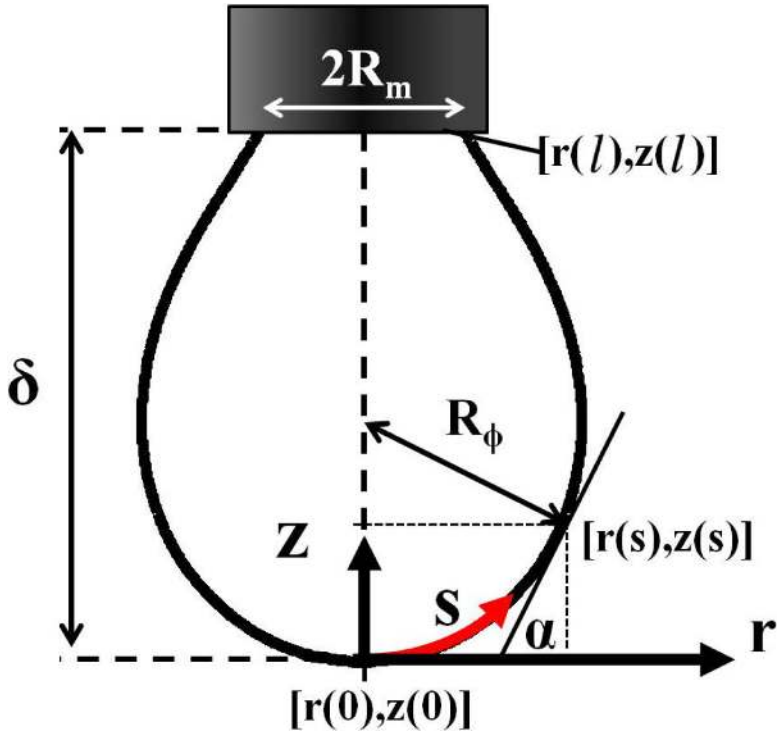

Figure 4.
Schematic representation of an axisymmetric pendant drop.

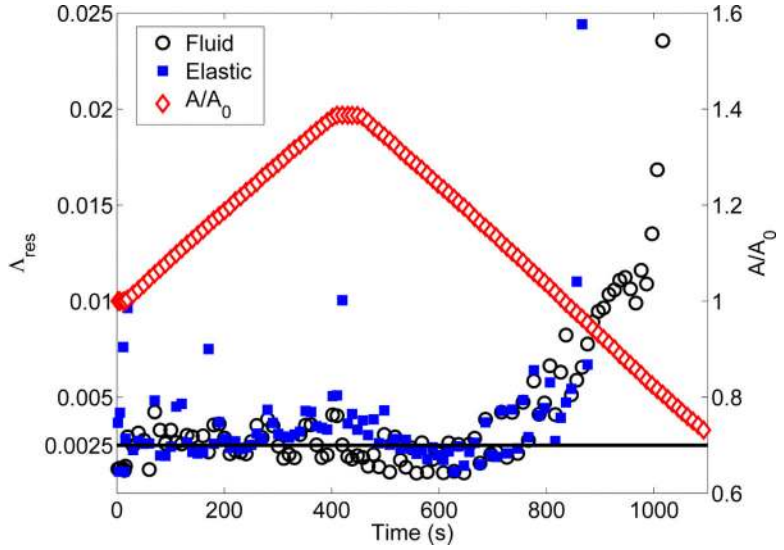

Figure 5.

Left axis: The fitting error, Λ_{res}, for the fluid and elastic analysis fits to the pendant drop profile. This measurement was the first expansion-compression cycle of an ionically crosslinked G92 membrane (20 minute incubation period). The solid black line corresponds to the average fitting error for the uncrosslinked G92 pendant drop. Right axis: Areal dilatation versus experiment time.

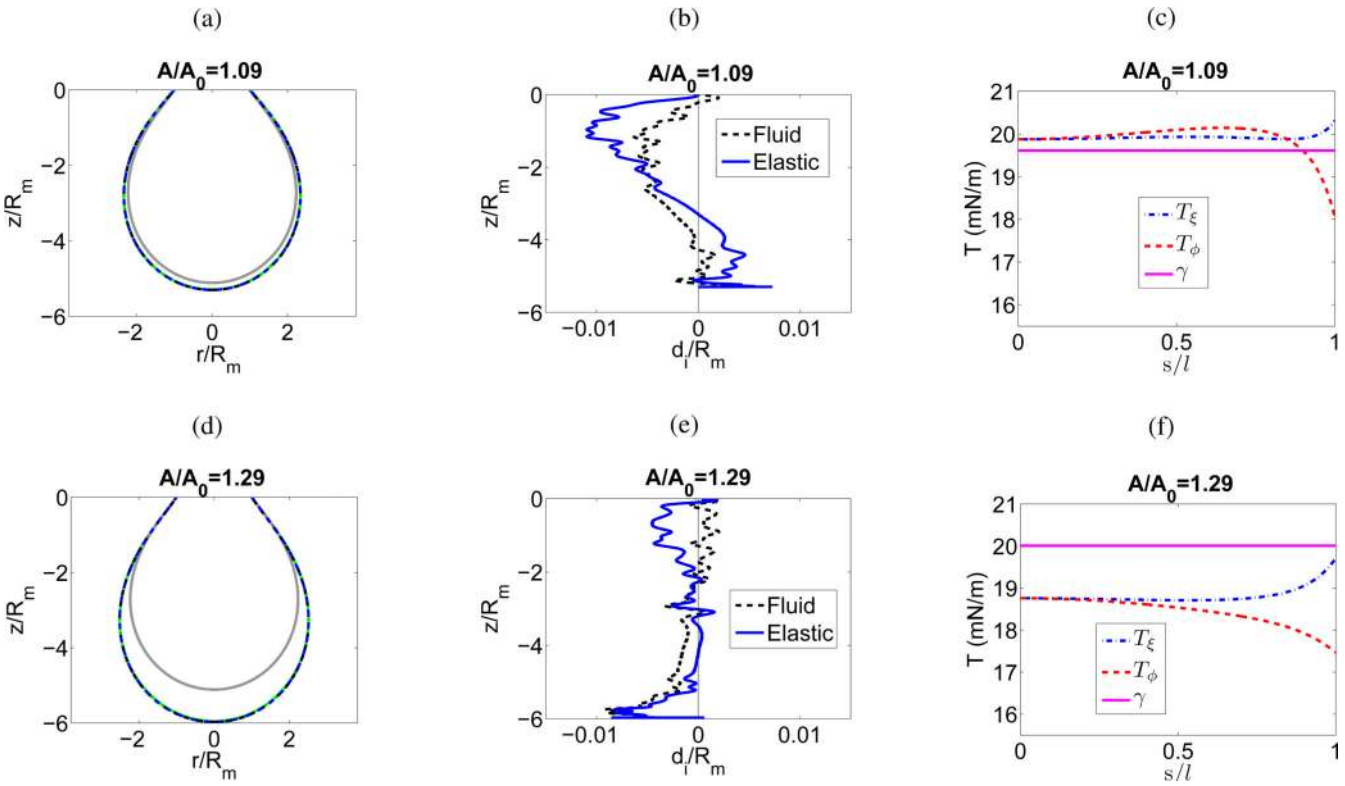

Figure 6.

Fluid and elastic interface analysis results for the first expansion/compression cycle of a G92 copolymer membrane (20 minute incubation time). Plots (a-c) correspond to A/A_0=1.09, time=110s. Plots (d-f) correspond to A/A_0=1.29, time=548s. Left plots (a,d) show the measured membrane profile prior to expansion (undeformed membrane, gray solid line) and the experimentally measured membrane profile at A/A_0 (deformed membrane, green solid line). The fluid model fit to the deformed membrane profile (black dashed line), and the elastic model fit to the deformed membrane profile (blue dashed line) are nearly indistinguishable from themselves and the measured deformed membrane profile. Center plot (b,e), shows the residual errors d_i/R_m, along the membrane profile from the fluid and elastic interface analysis. Right plots (c,f) compare the principal tensions given by the elastic analysis, to the interfacial tension, γ, measured with the fluid analysis. Note that these x-axes run from the membrane apex, $s/l = 0$, to the clamp edge, $s/l = 1$.

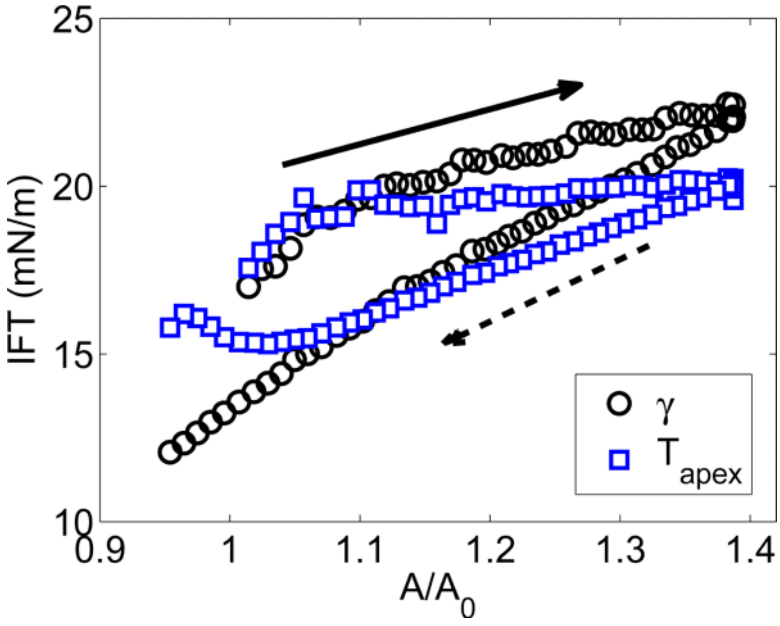

Figure 7.

Apex interfacial tension (IFT) plotted as function of areal dilatation for the first expansion/compression cycle of a crosslinked G92 copolymer membrane (20 minute incubation time). The solid arrow represents the direction of curve during expansion and the dashed arrow represents the direction of the curve during compression. The fluid interface analysis was used to calculate γ, and the elastic interface analysis was used to calculate the tension at the apex. Note $T_{\xi}(s = 0) = T_{\varphi}(s = 0) = T_{apex}$.

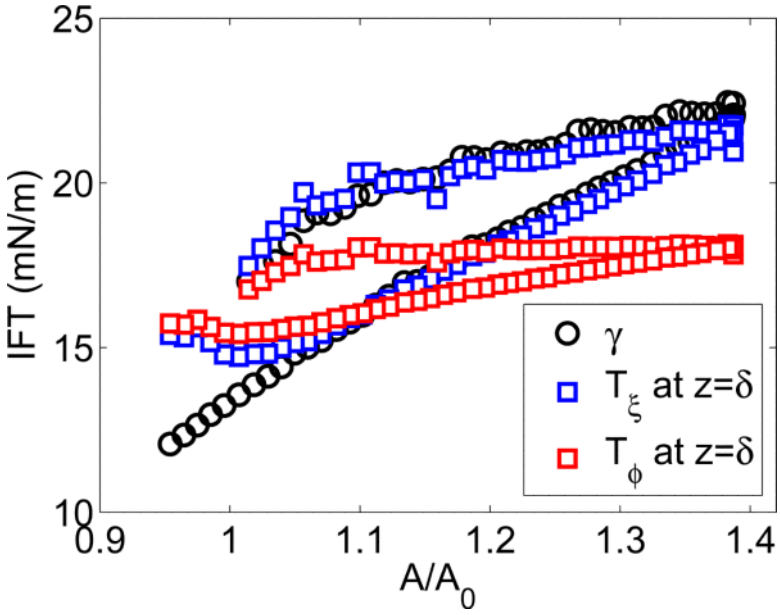

Figure 8.

Interfacial tension (IFT) at the capillary edge ($z(s = 1) = \delta$) plotted as a function of areal dilatation for the first expansion/compression cycle of a crosslinked G92 copolymer membrane (20 minute incubation time). The fluid interface analysis was used to calculate γ, and the elastic interface analysis was used to calculate the principal tensions at the capillary edge.

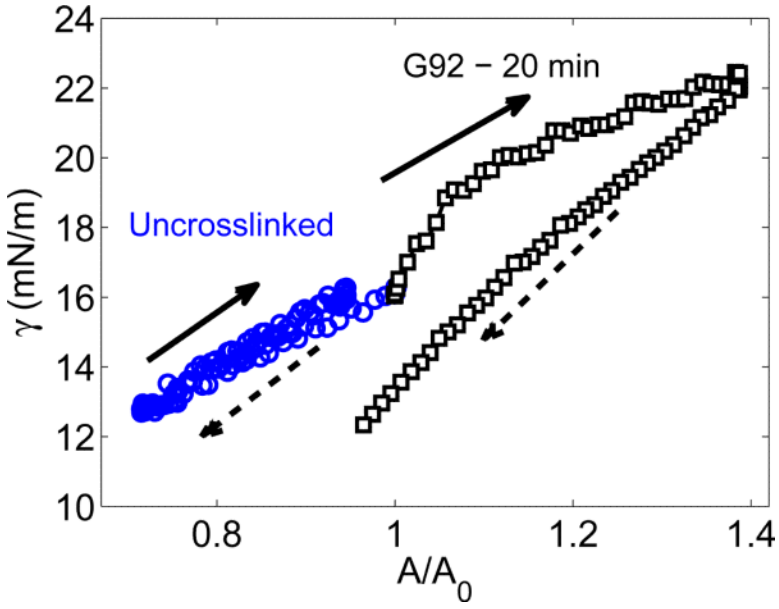

Figure 9.

Comparison of interfacial tension behavior between G92 uncrosslinked (blue circles) and crosslinked (black squares) layers during expansion/compression. Dashed arrows represent the direction of curve during compression and solid arrows represent the direction of the curve during expansion.

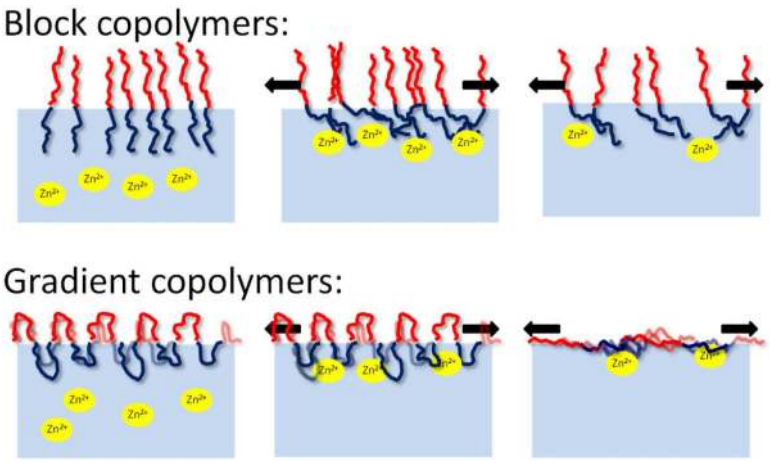

Figure 10.

Schematic illustration of the proposed interfacial structure evolution of crosslinked block and gradient copolymer membranes under an applied tensile force.

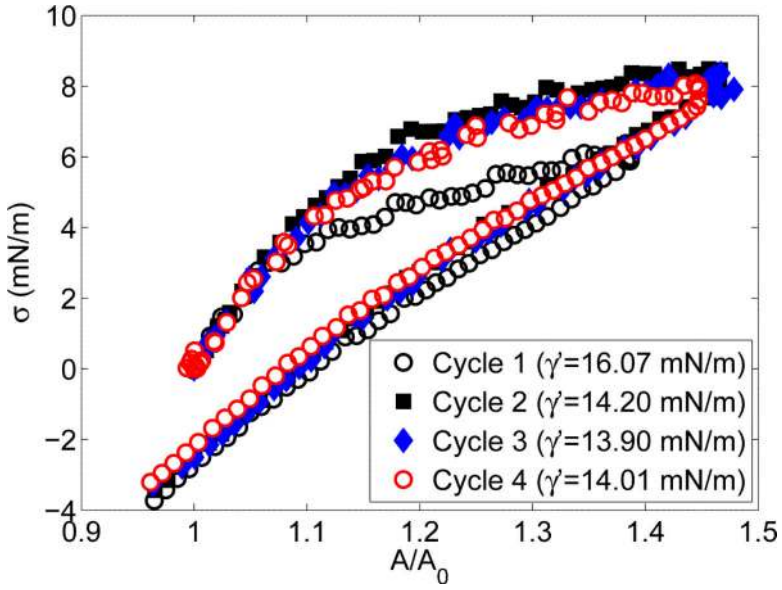

Figure 11.

Sequential expansion-compression cycles of G92 ionically crosslinked pendant drops (20 minute incubation time). The time between each cycle was approximately three minutes.

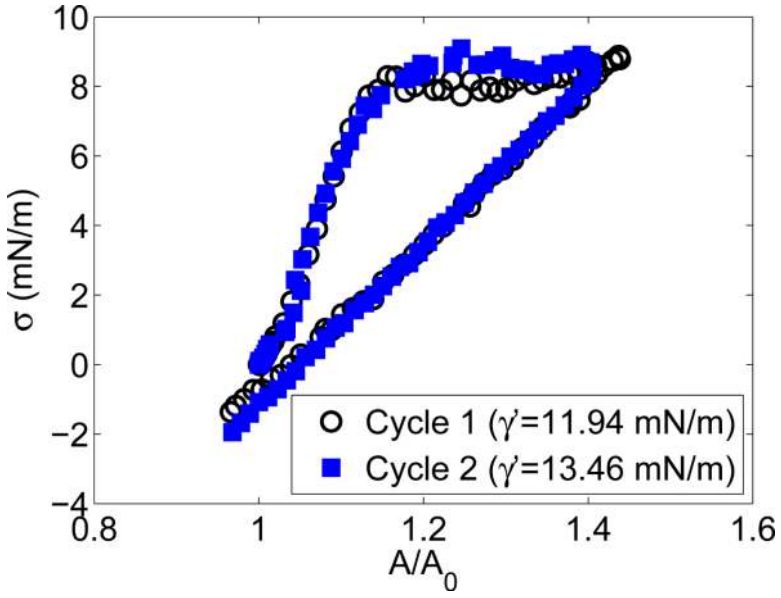

Figure 12.

Sequential expansion cycles of G92 ionically crosslinked pendant drops (30 minute incubation time). The time between cycles was approximately three minutes.

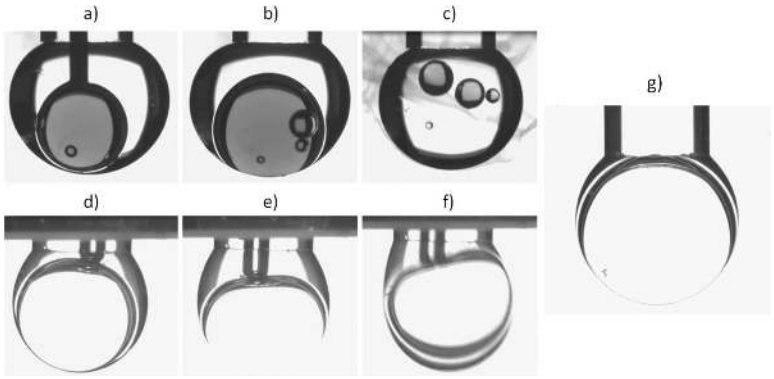

Figure 13.

(a-c): Images taken of a water drop placed inside an oil pendant drop containing uncrosslinked gradient copolymers (embedding phase is water). In less than two seconds, the inside water drop contacts the aqueous interface and bursts out. (d-f) If gradient copolymers are first crosslinked at the outer interface, the inside water droplet can be punched hard into the interface without breaking it. (g)As the chloroform phase evaporates, the inner water drop gets full contact with the original interface. The crosslinked membrane now becomes a barrier between a water/water interface.

Table 1

Summary of Molecular Characterization Data for Gradient (G) and Diblock (B) S/AA Copolymers

Sample	F_s	M_n(g/mol)[a]	PDI[a]
G92	0.55	91,800[b]	1.48[b]
B89	0.69	88,700[d]	1.79[b]

[a] Mn and PDI data based on S/tBA copolymers.

[b] Apparent value characterized relative to PS standards by GPC with THF as eluent.

[d] Mn value was determined from the M_n of PtBA macroinitiator and the F_S value.